Check for
updates

Experimental and smoothed particle hydrodynamics analysis of interfacial bonding between aluminum powder particles and aluminum substrate by cold spray technique

Abreeza Manap [1] · Tomonaga Okabe [2] · Kazuhiro Ogawa [3] · Savisha Mahalingam [1] · Huda Abdullah [4]

Abstract

This study aims on the dominant bonding mechanism between aluminum powder particles and aluminum substrate evaluated both experimentally and numerically. Aluminum particles were deposited at different velocities onto an aluminum substrate by cold spray (CS) technology. The crater, bond, and interface morphology upon impact were characterized using scanning electron microscopy, focused ion beam processing, and transmission electron microscopy. Experimental results reveal that rebound phenomenon existed at high velocities and excellent contact is obtained above the critical velocity. This denotes that ideal deposition occurs at a certain particle velocity scale. Meanwhile, the numerical analysis was performed via smoothed particle hydrodynamics (SPH) method. The simulated particle deformation behavior agreed well with the experimentally evaluated impact morphology, which confirms the viability of the SPH procedure for CS simulation. Furthermore, the numerically calculated deposition range was in correspondence with the experimental findings. The analysis demonstrates that interfacial bonding between the powder particles and substrate is influenced by the adhesive intersurface forces of the contacting surfaces.

Keywords Cold spray · Bonding · Impact behavior · Modeling · Smoothed particle hydrodynamics

1 Introduction

Cold spray (CS) technology made its first breakthrough in the mid-1980s by the Russian scientists in Novosibirsk. CS process utilizes metal powder particles to form a uniform coating on a substrate. The metal powders (typically 5 to 100 μm in particle size) are injected into a supersonic inert gas through impaction process [1]. The solid particles undergo plastic deformation and attach with the substrate upon impact.

✉ Abreeza Manap
abreeza@uniten.edu.my

1 Institute of Sustainable Energy, Universiti Tenaga Nasional, Jalan IKRAM-UNITEN, 43000 Kajang, Selangor, Malaysia

2 Department of Aerospace Engineering, Tohoku University, 6-6-1, Aoba, Aramaki-aza, Aoba-ku, Sendai, Miyagi 980-8579, Japan

3 Fracture and Reliability Research Institute, Graduate School of Engineering, Tohoku University, 6-6-1, Aoba, Aramaki-aza, Aoba-ku, Sendai, Miyagi 980-8579, Japan

4 Department of Electrical, Electronic and System Engineering, Faculty of Engineering and Built Environment, Universiti Kebangsaan Malaysia, 43600 Bangi, Selangor, Malaysia

Successive impacts result in a steady coating consisting of least porosity and excellent bond strength [1].

Kinetic energy depleted in the form of plastic dissipation energy generates high strain of plastic deformation, which is focused within the shear zone at the particle/substrate interface. This plastic dissipation energy is then converted into heat energy, which results in a local temperature rise in this small contact area. This in turn causes thermal softening and localized plastic deformation where the particles will be bonded successfully on the substrate when the particle velocity is higher than the critical velocity [2]. Grujicic et al. [3, 4] and Assadi et al. [5] have considered adiabatic shear instability and thermal softening to be two of the major bonding mechanisms.

However, there are fewer agreements on the most dominant mechanism in interfacial reaction. For instance, studies [5–10] have revealed the possibility of the occurrence of interfacial melting as a result of localized heating and how it may result in reliable metallurgical bonding. On the other hand, several research groups [3, 4, 11, 12] argued that while interfacial melting may occur through atomic diffusion, the high bond strengths measured in CS coatings cannot be solely attributed to it. Thus, the arguments prevail that melting may not play an

important role in interfacial reaction. Despite the various researches on CS, the real mechanism of particle deformation and bonding remains unexplained.

Therefore, simulated techniques are optimally adapted for CS interfacial mechanism because they enable a better analysis of particle/substrate deformation behavior and a more accurate estimation of critical velocity through numerical method of the entire particle/substrate impact and deformation process. In order to study on CS bonding, previous simulations implemented Lagrangian and Euler codes such as finite element methods (FEM) [5–9] and finite difference methods (FDM) [3, 4, 12], respectively. However FDM and FEM methods faced many challenges. For example, FDM encountered trouble in trailing free surfaces and mobile interfaces, and FEM experienced invalid results and early end in the simulation [13, 14]. To overcome these problems, Li et al. [13, 14] employed the Arbitrary Lagrangian-Eulerian method used in ABAQUS that involves both pure Lagrangian and pure Eulerian analyses to perform 2D and 3D modeling of CS particle impacts. Although a satisfactory output was obtained for the 3D models, the results from 2D models yielded unrealistic interface deformations. Furthermore, satisfactory results for the 3D models could only be obtained by incorporating material damage in the simulation. This simulation setting was however unavailable for the 2D model [14].

Within the last decade, several studies have been carried out by incorporating smoothed particle hydrodynamics (SPH) process for facile interfacial bonding mechanism [15–18]. SPH employs Lagrangian codes without the influence of mesh and favorable for hypervelocity impact simulation. SPH is a promising alternative to the conventional simulation process for CS bonding mechanism due to its mesh-free adaptation that minimizes great deformation drawbacks. In the previous literature [15], SPH method was used to study on how oblique impact influences particle deformation. The paper outlined that the size of CS particles has no impact on particle deformation and compression ratio, which signifies the viability of SPH technique for CS mechanism. However, the work did not investigate on simulation of velocity impact on CS bonding behavior.

The focus of this study is to examine the dominant bonding mechanism in CS technique through both numerical simulation and experimental measurement. The numerical simulation modeled the impact of spherical aluminum powder particles bonding on an aluminum substrate over a wide range of velocities via SPH method. The reliability of the model was verified through CS experiments of single particle impact tests. The effect of velocity on the particle deformation behavior was analyzed and a rebound phenomenon similar to Wu et al. [19] was observed. The critical and maximum velocities were estimated with respect to these experimental and numerical analyses. The dominant bonding mechanism

was discussed based on the findings of these experiments and simulations.

2 Numerical method

The SPH modeling of the CS process was performed using a program that was written in FORTRAN. The numerical method employed in this work is modified from the previous work done by Randles et al. [18] to ease interaction between the particle and substrate. The Johnson-Cook plasticity model was applied to explain the plastic feedback of the materials that executes strain, thermal softening, and strain hardening [20].

2.1 SPH methodology

Instead of a mesh, SPH employs the kernel approximation method by representing it integrally for field function approximation [15–18]. The kernel approximation is showed as in the following equation.

$$\langle f(x) \rangle = \int_{\Omega} f\left(x^{'}\right) W\left(\frac{\left|x-x^{'}\right|}{h}\right) dx^{'}, \qquad (1)$$

where f is the arbitrary function of the three dimensional position vector x, Ω is the volume, $(x - x^{'})$ is the distance between the particle of evaluation x and any arbitrary particle x' in Ω [21], and W is the width of the smoothing kernel.

The obtained kernel approximation is resembled further though particle approximation by replacing the integral in Eq. (1) with summations of neighboring particles in the support domain. The particle approximation becomes

$$\langle f(x) \rangle \cong \sum_{i=1}^{N} m_i f_i W\left(\frac{\left|x-x^{'}\right|}{h}\right) / p_i. \qquad (2)$$

where m_i and ρ_i are mass and density of particle i, respectively, N is the number of particles [22] in the support domain, and h is the smoothing length.

The further approximated kernel approximation (Eq. (2)) uses a few different smoothing functions in order to satisfy the mathematical conditions where the interpolation kernel is interpreted as cubic B-spline as in the following equation.

$$W_4(\nu, h) = \frac{1}{\pi h^3} \begin{cases} \left(1 - \frac{3}{2}\nu^2 + \frac{3}{4}\nu^3\right) & 0 < \nu < 1 \\ \frac{1}{4}(2-\nu)^3 & 1 < \nu < 2 \\ 0 & \text{otherwise} \end{cases}, \qquad (3)$$

where $\nu = |x_j - x_i|/h$ and i and j are the neighboring particles.

The continuous sequence of mechanics in the SPH model is defined by the conservation equations described in the following equations. Equations 4, 5, and 6 explain the conservation of mass, momentum, and energy, respectively.

$$\rho_i = \sum_j m_j W_{ij} \tag{4}$$

$$\frac{dU_i}{dt} = -\sum_j \frac{m_j}{\rho_i \rho_j} (\sigma_j - \sigma_i).\nabla W_{ij} \tag{5}$$

$$\frac{dE_i}{dt} = -\sum_j \frac{m_j}{\rho_i \rho_j} (U_j - U_i).\sigma_i.\nabla W_{ij} \tag{6}$$

where ρ, U, E, σ, and t are the scalar density, velocity vector, specific internal energy, stress tensor, and time, respectively [20].

2.2 Modeling cold-sprayed deposition

Two-dimensional models were applied in CS deposition modeling. The size of the substrate was modeled as seven times greater than the diameter of the particle (25 μm) with stable spaces of x and y directions. The particles and substrate were maintained at uniform distance to avoid initial penetration. A wide range of velocities (500 to 1000 m/s) was used to impact powder particles onto the substrate.

The pressure for a solid follows the linear Mie-Grüneisen equation of state (EOS) as given in the following equation [18].

$$p(\rho, E) = \left(1 - \frac{1}{2}\Gamma\eta\right)p_H(\rho) + \Gamma\rho E; \tag{7}$$

$$p_H = \begin{cases} a_o\eta + b_o\eta^2 + c_o\eta^3, & \eta > 0 \\ a_o\eta, & \eta < 0 \end{cases}, \tag{8}$$

where $\eta = \rho/\rho_o - 1$ is the compression, ρ_o is the density of the shock disturbance, ρ and E are the density and the internal energy of the material behind the shock, respectively, subscript H is the Hugoniot curve, and Γ is the Grüneisen parameter. Meanwhile, the constants (a_o, b_o, and c_o) are associated to the intercept, c and slope; S of $U_s = c + SU_p$ curve is interpreted in the following equation.

$$a_o = \rho_o c^2, \qquad b_o = a_o[1 + 2(S-1)], \qquad c_o$$
$$= a_o\left[2(S-1) + 3(S-1)^2\right] \tag{9}$$

The yield stress was defined based on Johnson-Cook plasticity model [18, 23] giving

$$\sigma_Y = \left[A + B(\varepsilon_p)^n\right]\left[1 + C\ln\left(\dot{\varepsilon}_p/\varepsilon_0\right)\right]\left[1 - (T^*)^m\right] \tag{10}$$

where σ_Y, $\dot{\varepsilon}_p = (2/3)\sqrt{(3K_2)}$, K_2, ε_p, $\dot{\varepsilon}_0$, n, and A, B, C, and m are the yield stress, equivalent plastic strain rate, second invariant of the plastic strain rate tensor, time integral of $\dot{\varepsilon}_p$, reference strain rate, work hardening exponent, and constants, respectively. Whereas in the dimensionless temperature, T^* is given as $T^* = (T-T_0)/(T_m-T_0)$ where T, T_m, and T_0 are the temperature in kelvin, melting temperature of the material, and reference temperature, respectively [20]. Damage and fracture evolution is described by the Johnson-Cook damage model [23], which is formulated as a rate- and temperature-dependent model. Damage is defined as

$$D_s = \dot{\varepsilon}_p/\varepsilon_f \tag{11}$$

$$\varepsilon_f = \left[d_1 + d_2 exp(d_3\sigma^*)\right]\left[1 + d_4\ln\left(\dot{\varepsilon}_p/\varepsilon_0\right)\right]\left[1 + d_5 T^*\right] \tag{12}$$

where ε_f is the rupture strain and σ^* is the ratio of the mean stress $-p$ to the equivalent stress $\sqrt{3J_2}$ where J_2 is the second invariant of the deviatoric stress tensor. d_1–d_5 are constants and T^* is defined in the Johnson-Cook plasticity model.

In this study, aluminum was used as both powder particle and substrate. Table 1 lists the material properties [6, 14] and Grüneisen EOS constants [24].

2.3 Particle/substrate interaction

Figure 1 illustrates the coalescence process also known as interfacial bonding developed using cohesive zone model. This study implements Dugdale-Barenblatt cohesive zone model involving critical separation distance, δ_c. The primary parameters used to characterize the interfacial bonding have been described in the previous study [25].

3 Experiments

3.1 Cold spray process

The samples were produced using a high-pressure cold spray system: PCS-203 (Plasma Giken Kogyo Co. Ltd., Japan). The CS system utilizes a high-pressure gas source for both main flow and feedstock powder carrier flow. Helium and nitrogen gasses were streamed as process and carrier gas, respectively,

Table 1 The material properties and Grüneisen EOS constants used in the SPH model

Properties (unit)	Value
Density, ρ (kg/m^3)	2710
Shear modulus (GPa)	27.0
Heat capacity (J/kg/K)	904
Reference temperature, T_0 (K)	300
Melting temperature, T_m (K)	916
JC plasticity: A (MPa), B (MPa), C, N, m	148.4, 345.5, 0.001, 0.183, 0.895
JC damage: d_1, d_2, d_3, d_4, d_5	0.071, 1.248, −1.142, 0.147, 1.0
Gruneisen EOS: Γ, c (m/s), S	1.97, 5386, 1.339
Intersurface traction, F (N)	3×10^{-3}
Critical separation, δ_c (m)	2×10^{-7}

to provide broader scale of velocity ranging from 0.5 to 3 MPa with particle and substrate temperature of 300 K. The material used was pure aluminum (Al G-AT, Fukuda Metal Foil & Powder Corporation; 25 μm) and aluminum alloy (A1050) as the feedstock powder and substrate, respectively. The nozzle was transported in a single stroke across the substrate with standoff interval at 15 mm and the lowest powder feed rate (0.1 rpm) was used to allow limited deposition.

3.2 Microstructure investigation

Microstructural characterization of the surfaces of the coating specimen was performed using a scanning electron microscope (SEM): FE-SEM 4700 (Hitachi). Single powder particle deposition was mainly seen at the boundary region of the coating. The interface between particle and substrate was analyzed using a transmission electron microscope (TEM): HF-2000 (Hitachi). Before TEM observation, thin foils of samples sprayed using nitrogen gas at 2 MPa and helium at 2 and 3 MPa were prepared using focused ion beam processing (FIB).
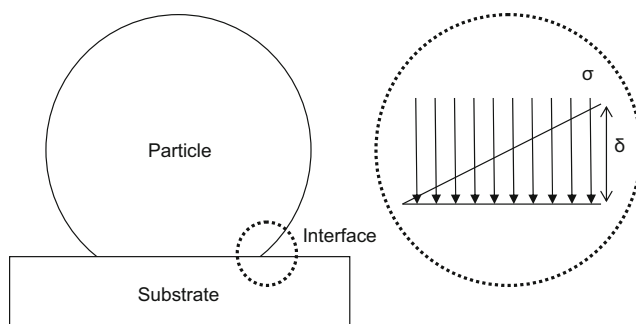
3.3 Particle velocity measurement

Particle image velocimetry (PIV) purchased from Seika Co. Ltd., Japan, was used to measure the particle velocities. The particle velocity is measured by displacement method where the particle in a target plane is displaced between two successive light pulses accompanied by a time delay. The location of particle and its mobility is recorded and analyzed through a digital camera with a charge-coupled device chip and image analysis software, respectively. In the present experiment, the powder particles were directly used for imaging and velocity calculation. The surrounding air was not seeded and no substrate was used in the experiment. The measuring domain was set as a central rectangular volume of 5 mm × 4 mm × 1 mm with its center at a vertical gap of 20 mm from the nozzle exit. The mean particle velocity was measured referring to the particle velocity distribution, which follows the Gaussian distribution, according to which the particle velocity in the central area is greater than the particle velocity in the boundary area of the measuring domain. Details of the procedure have been reported elsewhere [26, 27]. Table 2 shows the calculated mean particle velocities for nitrogen and helium as process gasses.

4 Results and discussion

4.1 Numerical results with no cohesive zone

Figure 2 shows the simulated temporal development obtained for the particle velocity and kinetic energy at velocity of 780 m/s with absence of cohesive zone. Upon impact, the kinetic energy from the initial velocity of the powder particle generates pressure at the particle/substrate interface, which causes the powder particle and the substrate to experience plastic deformation. During the impacting process, the kinetic energy of the powder particle dissipates into both the particle and the substrate, causing the particle velocity and kinetic

Fig. 1 Schematic diagram of the interfacial bonding between spherical particle and substrate due to adhesive intersurface forces

Table 2 The mean particle velocities for Ni and He process gas conditions

Gas	Pressure (MPa)	Particle velocity (m/s)	
		Central region	Boundary region
Helium	2.96	1169.6	870.2
	2.46	1088.8	841.0
	1.96	1026.4	780.7
	1.46	988.8	758.7
	0.96	926.3	744.9
Nitrogen	2.96	790.6	720.3
	1.96	696.5	692.8
	0.96	589.3	–
	0.46	558.4	–
	0.16	462.0	–

energy to decrease. The velocity and kinetic energy ultimately drop to zero, pressure at the interface decreases, and the deformation stops. These results are consistent with those observed for the CS particles in previous simulations [3–8]. However, a negative particle velocity is observed between 50 and 100 ns, which indicate rebound or non-adhesion of the powder particles.

Figure 3 shows the coefficient of restitution obtained at 550–1000 m/s with absence of cohesive zone (blue). The coefficient of restitution is the ratio of velocity after impact
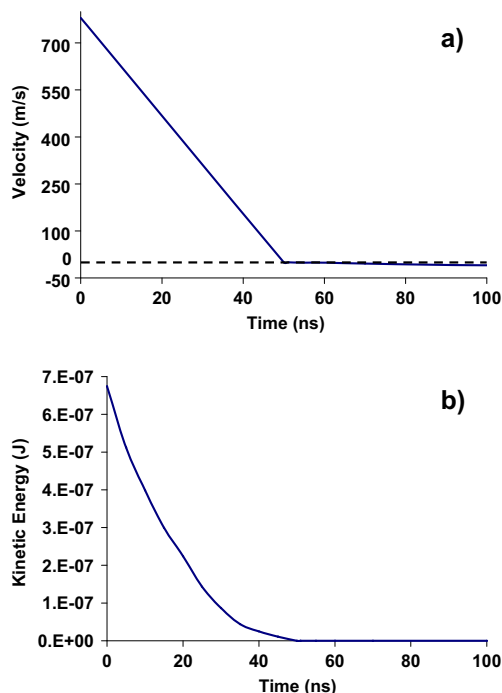
(rebound velocity) to the velocity before impact (particle velocity) and it decreases with increasing velocity until it reaches a minimum value at 780 m/s. The coefficient of restitution then increases with further increase in velocity. Figure 3 signifies that the particle will rebound at any velocity. To solve this problem, a cohesive zone with intersurface traction was incorporated into the numerical model.

4.2 Numerical results with cohesive zone

Figure 4 shows the deformation pattern at velocity of 700 m/s, 780 m/s, and 870 m/s with presence of cohesive zone. Upon impact, the particles deformed from spherical powder particles to flattened particles with formation of a crater. The flatness of the particles increased as the velocity increased from 700 to 870 m/s. Figure 4 is distinguished between blue (no damage) and red (damage) regions which indicate pure elastic zone and elastic plastic zone respectively. Damage is defined by Eq. (11) where the effective plastic strain exceeds the rupture strain. Intensive deformation is observed at the contact zone between the powder particle and substrate. Formation of a metal jet was also observed at the contact surface. These observations are similar to those reported in studies [5–9] using the FEM technique.

Figure 3 also illustrates the coefficient of restitution at velocity of 550–1000 m/s with presence of cohesive zone (red). From Fig. 3, the coefficient of restitution is zero from the critical velocity (650 m/s) until the maximum velocity (900 m/s). This result indicates that the rebound velocity is relatively very small compared to the particle velocity where the bonding between the particle and substrate has successfully occurred. Thus, particle velocity range of 650–900 m/s is the range for deposition of aluminum powder particles on the aluminum substrate. On the other hand, particles impacting at particle velocities below the critical velocity or above the
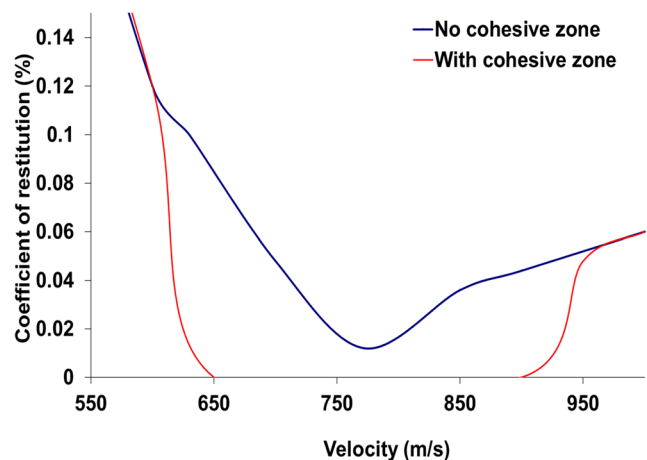
Fig. 2 The simulated temporal development for **a** particle velocity and **b** kinetic energy obtained from SPH for a 25 μm aluminum powder particle during impact onto the surface of a flat aluminum substrate at 780 m/s obtained with no cohesive zone

Fig. 3 The coefficient of restitution obtained from SPH for a 25 μm aluminum powder particle impacting onto the surface of a flat aluminum substrate at 550–1000 m/s with and without cohesive zone or intersurface traction at the particle/substrate interface
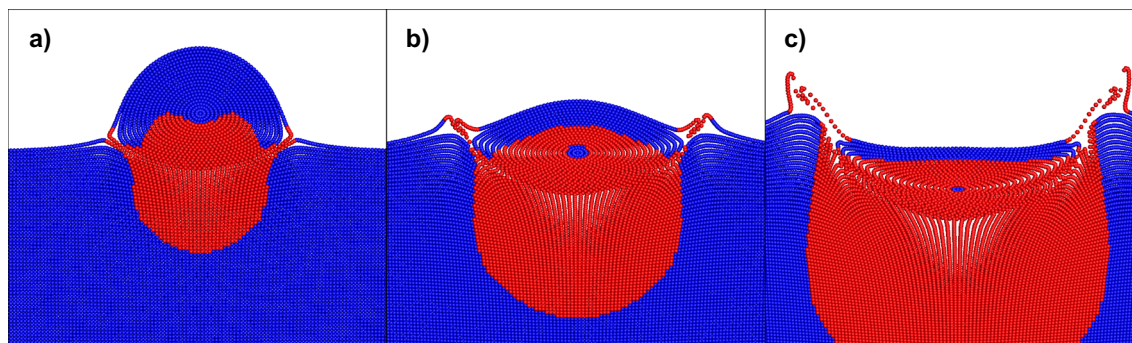
Fig. 4 SPH simulations of a 25 μm aluminum powder particle during impact onto the surface of a flat aluminum substrate with cohesive zone and intersurface traction at the particle/substrate interface. The deformation patterns obtained at particle velocities **a** 650 m/s, **b** 780 m/s, and **c** 900 m/s. The temperature contours obtained at particle velocities **d** 650 m/s, **e** 780 m/s, and **f** 900 m/s

maximum velocity are rebounded. This rebound phenomenon [19] can be explained as follows.

When a powder particle impacts on a substrate, the initial kinetic energy is dissipated within the particle and into the substrate as plastic dissipation energy, and generates plastic deformations that are concentrated within a small contact zone. The remaining kinetic energy is then stored in the pure elastic region as elastic energy which is later transferred back into the particle as kinetic energy, resulting in rebound of the particles. At impact velocities above the critical velocity, material loses potential to store elastic energy due to large plastic deformation and thermal softening [28]. This enables deposition of particles on the substrate. At impact velocities above the maximum velocity, the deformed particles are once again reflected off the substrate. When thermal softening starts, the maximum particle deformation is reached and the plastic zone is toughen resulting in a new elastic stress limit, also referred to as the secondary elastic stress limit [29]. It is possible that the excess kinetic energy is then stored as elastic energy in this new elastic region instead of further dissipating into the substrate and later transferred back into the particle as kinetic energy, resulting in rebound of the particles. Therefore, the rebound phenomenon and the deformation behavior of rebounded particles can only be analyzed by simulation process, highlighting the significance and fitness of numerical method in solving impact issues.

4.3 Comparison between experimental and numerical results

Figure 5 shows the SEM images obtained from the experiments for the bonded splats (45° tilted view) of a 20–30 μm aluminum powder particle impacted onto a flat aluminum substrate at 693 m/s, 781 m/s, and 870 m/s. The results show that the plastic deformation occurred in the particle and substrate increased as the particle velocity increased. Figure 5 agrees well with the SPH simulations in Fig. 4. For further analysis, the bond ratio was calculated by evaluating the impacted surface of the substrate. The bond ratio or deposition

efficiency is the ratio of bonded particles to total sprayed particles in a unit area of impact surface [19]. The bond ratio has been presented in Fig. 6. The particles rebounded at low and high velocities resulting in a low bond ratio show the presence of a rebound event. The particle velocities where the bond ratio is predicted to become zero are taken as the values of critical and maximum velocities. The estimated critical and maximum velocities are 680 m/s and 880 m/s, respectively, which define the particle velocity range for deposition. Furthermore, a maximum bond ratio existed in the middle of the range (780 m/s), which indicates that maximum deposition is obtained at the mean particle velocity. Besides that, the maximum deposition value of 780 m/s is almost similar to the theoretical critical velocity of 775 m/s of aluminum particle (25 μm).

Figure 6 agrees well with the particle velocity range for deposition obtained numerically in Fig. 3 with cohesive zone (red). The numerically evaluated particle velocity range (650–900 m/s) is slightly larger as compared to the experimentally evaluated particle velocity range (680–880 m/s). Kang et al. [26] found that the oxygen scale on the particle surface of the aluminum powder can influence the bond ratio, and increasing the oxygen content may decrease the bond ratio. Therefore, the smaller particle velocity range obtained from the experiment is assigned to the oxygen content in the powder.

The bonded interface has been analyzed in detail. The Fresnel contrast image of the Al-Al interface of a powder particle impacted onto a flat aluminum substrate at 780 m/s is given in Fig. 7. This contrast mode can be used to study the interface using TEM. For perfectly abrupt interfaces, a residual Fresnel contrast and discontinuity can be observed. This, however, was not detected in Fig. 7, which demonstrates the diffuseness of the interface.

4.4 Deposition mechanism

Surface adhesion driven by the intersurface forces is proposed to be the deposition mechanism. A good adhesion reflects to the clean surfaces and high contact

Fig. 5 SEM images obtained from the experiments for the bonded splats (45° tilted view) of a 20–30 μm aluminum powder particle impacted onto the surface of a flat aluminum substrate at particle velocities **a** 693 m/s, **b** 781 m/s, and **c** 870 m/s
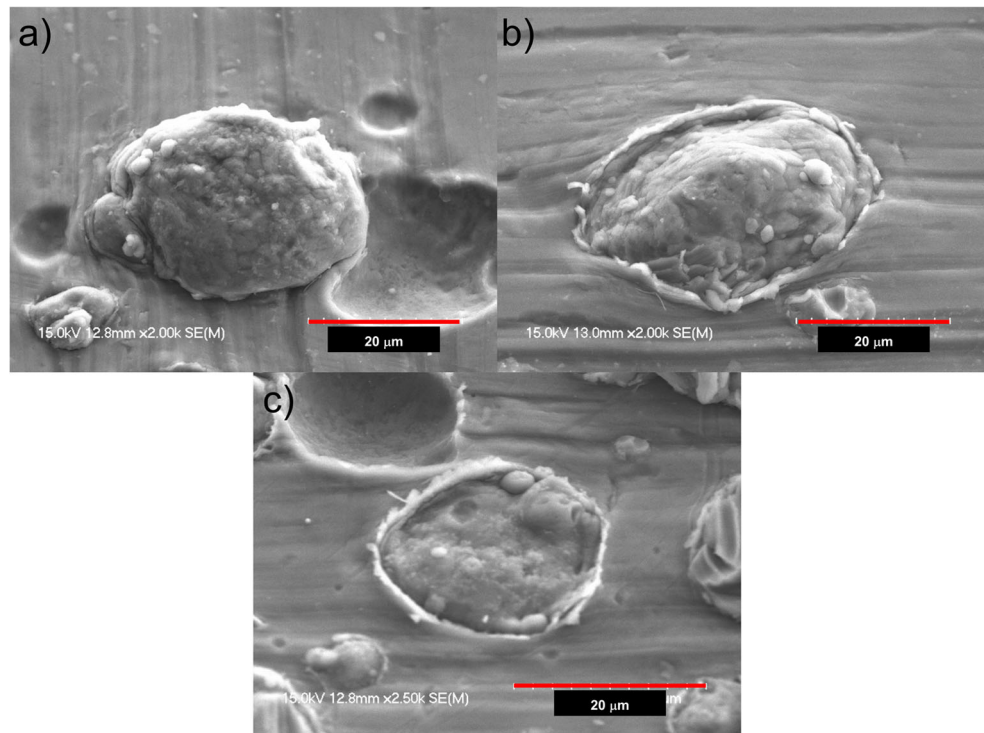
pressures. Thus, the formation of a mutually conforming contact surface is a signal to attractive atomic interaction. This attractive atomic interaction was translated to a larger scale and modeled in SPH as the forces acting at the contact surface upon impact. The results obtained using SPH agrees well with the experimental results. From the experiments, the diffusiveness of the particle and the substrate, determined through the residual Fresnel contrast observation using TEM, demonstrates the formation of a mutually conforming contact surface. Furthermore, in our previous study [25], deposition efficiency was found to be

higher for coatings with better adhesion property. Based on the results of this study, interfacial bonding is driven by the intersurface forces that act within the cohesive region. Although the formation of large intermetallic phases and thus high bonding strengths observed in the previous studies [8–10] is said to be only possible with the presence of liquid, interfacial bonding observed in studies [3, 12] where melting was not found can be attributed to the adhesive intersurface forces at the contacting surfaces.
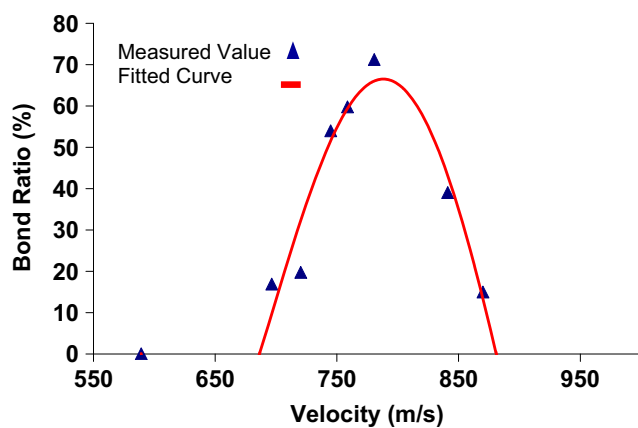

Fig. 6 Bond ratio obtained from the experiments for the bonded splats of a 20–30 μm aluminum powder particle impacted onto the surface of a flat aluminum substrate at particle velocities 550–1000 m/s
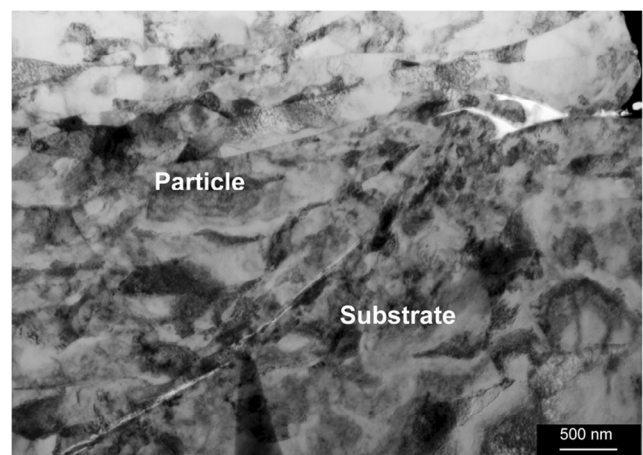

Fig. 7 The Fresnel contrast image obtained from the experiments for the Al-Al interface of a 20–30 μm aluminum powder particle impacted onto the surface of a flat aluminum substrate at a particle velocity of 780 m/s

5 Conclusion

In summary, the interfacial bonding mechanism between aluminum powder particles and aluminum substrate was successfully studied using SPH numerical method accompanied by experimental measurements. The viability of SPH method for studying the impact behavior in CS was proven in this work where the deposition mechanism corresponds well with experimental findings. Moreover, a rebound event was found indicating presence of a certain particle velocity range for deposition of particle onto the substrate. This shows the feasibility of SPH method as a convenient implementation to predict critical and maximum velocities for deposition and optimize spray conditions for various materials. In addition to the thermal softening and adiabatic shear instability, the adhesive intersurface forces at the contacting surfaces as well as the work of adhesion play a significant role in the impact behavior between the powder particles and the substrate.

References

1. Nélias D, Xie J, Walter-Le Berre H, Ichikawa Y, Ogawa K (2014) Simulation of the cold spray deposition process for aluminum and copper using Lagrangian, ALE and CEL methods. In: Jean MB (ed) Thermomechanical industrial processes: modeling and numerical simulation. Wiley, pp 321–358

2. Kim J, Lee C (2016) Correlation of impact conditions, interface reactions, microstructural evolution, and mechanical properties in kinetic spraying of metals: a review. J Therm Spray Technol 25: 1461–1489. https://doi.org/10.1007/s11666-016-0448-y

3. Grujicic M, Saylor JR, Beasley DE, DeRosset WS, Helfritch D (2003) Computational analysis of the interfacial bonding between feed-powder particles and the substrate in the cold-gas dynamic-spray process. Appl Surf Sci 219:211–227. https://doi.org/10.1016/S0169-4332(03)00643-3

4. Grujicic M (2007) Particle/substrate interaction in the cold-spray bonding mechanism. Woodhead Publishing Ltd, London

5. Assadi H, Gartner F, Stoltenhoff T, Kreye H (2003) Bonding mechanism in cold gas spraying. Acta Mater 51:4379–4394. https://doi.org/10.1016/S1359-6454(03)00274-X

6. Bae G, Xiong Y, Kumar S, Kang K, Lee C (2008) General aspects of interface bonding in kinetic sprayed coatings. Acta Mater 56: 4858–4868. https://doi.org/10.1016/j.actamat.2008.06.003

7. Bae G, Kumar S, Yoon S, Kang K, Na H, Kim HJ, Lee C (2009) Bonding features and associated mechanisms in kinetic sprayed titanium coatings. Acta Mater 57:5654–5666. https://doi.org/10.1016/j.actamat.2009.07.061

8. King PC, Bae G, Zahiri SH, Jahedi M, Lee C (2010) An experimental and finite element study of cold spray copper impact onto two aluminum substrates. J Therm Spray Technol 19:620–634. https://doi.org/10.1007/s11666-009-9454-7

9. Guetta S, Berger MH, Borit F, Guipont V, Jeandin M, Boustie M, Poitiers F, Ichikawa Y, Ogawa K (2009) Influence of particle velocity on adhesion of cold-sprayed splats. J Therm Spray Technol 18:331–342. https://doi.org/10.1007/s11666-009-9327-0

10. Barradas S, Guipont V, Molins R, Jeandin M, Arrigoni M, Boustie M, Bolis C, Berthe L, Ducos M (2007) Laser shock flier impact simulation of particle-substrate interactions in cold spray. J Therm Spray Technol 116:548–556. https://doi.org/10.1007/s11666-007-9069-9

11. Wu J, Yang J, Fang H, Yoon S, Lee C (2006) The bond strength of Al–Si coating on mild steel by kinetic spraying deposition. Appl Surf Sci 252:7809–7814. https://doi.org/10.1016/j.apsusc.2005.09.015

12. Dykhuizen RC, Smith MF, Gilmore DL, Neiser RA, Jiang X, Sampath S (1999) Impact of high velocity cold spray particles. J Therm Spray Technol 8:559–564. https://doi.org/10.1361/105996399770350250

13. Li WY, Liao H, Li CJ, Li G, Coddet C, Wang X (2006) On high velocity impact of micro-sized metallic particles in cold spraying. Appl Surf Sci 253:2852–2862. https://doi.org/10.1016/j.apsusc.2006.05.126

14. Li WY, Gao W (2009) Some aspects on 3D numerical modeling of high velocity impact of particles in cold spraying by explicit finite element analysis. Appl Surf Sci 255:7878–7892. https://doi.org/10.1016/j.apsusc.2009.04.135

15. Li WY, Shuo Y, Wang XF (2010) Numerical investigations of the effect of oblique impact on particle deformation in cold spraying by the SPH method. Appl Surf Sci 256:3725–3734. https://doi.org/10.1016/j.apsusc.2010.01.014

16. Liu MB, Liu GR, Zong Z, Lam KY (2003) Computer simulation of high explosive explosion using smoothed particle hydrodynamics methodology. Comput Fluids 32:305–322. https://doi.org/10.1016/S0045-7930(01)00105-0

17. Hiermaier S, Konke D, Stilp AJ, Thoma K (1997) Computational simulation of the hypervelocity impact of Al-spheres on thin plates of different materials. Int J Impact Eng 20:363–374. https://doi.org/10.1016/S0734-743X(97)87507-0

18. Randles PW, Libersky LD (1996) Smoothed particle hydrodynamics: some recent improvements and applications. Comput Method Appl Mech Engl 139:375–405. https://doi.org/10.1016/S0045-7825(96)01090-0

19. Wu J, Fang HY, Yoon SH, Kim HJ, Lee C (2006) The rebound phenomenon in kinetic spraying deposition. Scr Mater 54:665–669. https://doi.org/10.1016/j.scriptamat.2005.10.028

20. Manap A, Okabe T, Ogawa K (2011) Computer simulation of cold sprayed deposition using smoothed particle hydrodynamics. Procedia Eng 10:1145–1150. https://doi.org/10.1016/j.proeng.2011.04.190

21. Jonsén P, Pålsson BI, Häggblad HÅ (2012) A novel method for full-body modelling of grinding charges in tumbling mills. Miner Eng 33:2–12. https://doi.org/10.1016/j.mineng.2012.01.017

22. Liu MB, Liu GR (2006) Restoring particle consistency in smoothed particle hydrodynamics. Appl Numer Math 56:19–36. https://doi.org/10.1016/j.apnum.2005.02.012

23. Johnson GR, Cook WH (1983) A constitutive model and data for metals subjected to large strains, high strain rates, and high temperatures. In: Proceedings of the 7th International Symposium on Ballistics. Hague (Netherlands), pp 541–547

24. Akarca SS, Song X, Altenhoff WJ, Alpas AT (2008) Deformation behaviour of aluminium during machining: modelling by Eulerian and smoothed-particle hydrodynamics methods. Proc IMechE L J Mater Des Appl 222:209–221. https://doi.org/10.1243/14644207JMDA187

25. Manap A, Nooririnah O, Misran H, Okabe T, Ogawa K (2014) Experimental and SPH study of cold spray impact between similar and dissimilar metals. Surf Eng 30(5):335–341. https://doi.org/10.1179/1743294413Y.0000000237

26. Kang K, Yoon S, Ji Y, Lee C (2008) Oxidation dependency of critical velocity for aluminum feedstock deposition in kinetic

spraying process. Mater Sci Eng A-Struct 486:300–307. https://doi.org/10.1016/j.msea.2007.09.010

27. Lee J, Shin S, Kim HJ, Lee C (2007) Effect of gas temperature on critical velocity and deposition characteristics in kinetic spraying. Appl Surf Sci 253:3512–3520. https://doi.org/10.1016/j.apsusc.2006.07.061

28. Klinkov SV, Kosarev VF, Rein M (2005) Cold spray deposition: significance of particle impact phenomena. Aerosp Sci Technol 9:582–591. https://doi.org/10.1016/j.ast.2005.03.005

29. Xu M, Willeke K (1993) Right-angle impaction and rebound of particles. J Aerosol Sci 24:19–30. https://doi.org/10.1016/0021-8502(93)90082-K